

Martingale deep learning for very high dimensional quasi-linear partial differential equations and stochastic optimal controls ^{*}

Wei Cai[†], Shuixin Fang[‡], Wenzhong Zhang[§], Tao Zhou[‡]

Abstract

High-dimensional parabolic partial differential equations (PDEs) often involve large-scale Hessian matrices, which are computationally expensive for deep learning methods relying on automatic differentiation to compute derivatives. This work aims to address this issue. In the proposed method, the PDE is reformulated into a martingale formulation, which allows the computation of loss functions to be derivative-free and parallelized in time-space domain. Then, the martingale formulation is enforced using a Galerkin method via adversarial learning techniques, which eliminate the need of computing conditional expectations in the martingale property. This method is further extended to solve Hamilton-Jacobi-Bellman (HJB) equations and the associated Stochastic optimal control problems, enabling the simultaneous solution of the value function and optimal feedback control in a derivative-free manner. Numerical results demonstrate the effectiveness and efficiency of the proposed method, capable of solving HJB equations accurately with dimensionality up to 10,000.

Keywords: Hamilton-Jacobi-Bellman equation, high dimensional PDE, stochastic optimal control, adversarial networks, martingale formulation

1 Introduction

High-dimensional partial differential equations (PDEs) are encountered in various fields, including quantum physics, system controls, financial engineering, and data science, where traditional numerical methods become infeasible due to the curse of dimensionality (CoD) [4]. In recent years, the introduction of deep learning into numerical method designs has led to some groundbreaking advances in tackling the CoD, yielding practical approaches for high-dimensional PDEs. These approaches can be broadly classified into two categories:

- Direct approach: neural networks are trained to learn the solutions of the PDEs, as exemplified by the Physics-Informed Neural Networks (PINNs) [10; 16; 19; 29; 33], Deep Galerkin Method (DGM) [1; 32], Deep Ritz [9], Weak Adversarial Networks (WANs) [35], etc.
- Stochastic differential equation (SDE)-based approach: the PDE is reformulated into a SDE model and then solved by deep learning. Relevant works include the

^{*}This work of SF and TZ is supported by the NSF of China (under grant 12288201) and the Youth Innovation Promotion Association (CAS). WZ is supported by the National Key R&D Program of China (under grant 2022YFA1005203) and the NSF of China (under grant 92270205, grant 1220012530). Date: August 26, 2024. The work of WC is funded by Clements Chair of Applied Math. at SMU.

[†]Department of Mathematics, Southern Methodist University. Email: cai@smu.edu.

[‡]Institute of Computational Mathematics and Scientific/Engineering Computing, Academy of Mathematics and Systems Science, Chinese Academy of Sciences.

[§]Suzhou Institute for Advanced Research, University of Science and Technology of China.

DeepBSDE [8; 13; 14], Forward-Backward Stochastic Neural Networks [30; 36], deep splitting method [3], deep backward schemes [11; 21], Actor-critic method [37], deep neural networks algorithms [2; 20], diffusion loss [26], diffusion Monte Carlo like approach [15], etc.

When applied to high-dimensional PDEs, the above two approaches enjoy different features. In the direct approach, the empirical loss for the neural network training is generally computed over a set of randomly sampled points in the solution domain. A useful merit of this approach is that computations for the sampled points are decoupled and thus amenable to parallel computing. However, this approach typically relies on automatic differentiation to compute the derivatives in the PDE, which can be quite expensive when the equation is truly high-dimensional and involves Hessian matrices with $d \times d$ entries. To address this issue, a stochastic dimension gradient descent (SDGD) implementation of PINNs was recently proposed to solve some very high-dimensional PDEs [19].

In contrast to the direct approach, the stochastic differential equation model-based approach can avoid the expensive computation of second-order derivatives in the original PDEs by recasting the problem into a stochastic framework. However, learning stochastic models introduces new difficulties that do not appear in the direct approach: i) Most SDE-based methods, such as [8; 13; 14; 15; 26; 30; 36; 37], rely on simulating sample paths. When applied to quasilinear parabolic PDEs (see, Eq. (1)) or HJB equations (see Eq. (23)), these sample paths depend on the unknown solution or optimal control being learned, requiring iterative updates throughout the training process. These updates are sequential in time and significantly increases computational costs. ii) The SDE-based methods [2; 3; 11; 20; 21] propose to solve the problems backwardly in time, which can reduce training difficulty, but limits the time parallelizability of the algorithm.

In addition to conventional high-dimensional PDEs, this work consider particularly Hamilton-Jacobi-Bellman (HJB) equations, which arise from dynamic programming methods for stochastic optimal control problems (SOCs). The HJB equation for SOCs contains second-order derivatives and is typically very high-dimensional, since real-world stochastic problems frequently involve numerous state and control variables. Moreover, a unique challenge in solving the HJB equation lies in the embedded minimization problem (see Eq. (23)), where the minimizer generally has no analytic expression, and the SDGD version of PINN is no longer applicable. Conventional PDE solvers need to find the minimizer for each time-space point, leading to high computational costs. To address this issue, a popular method is the policy improvement algorithm (PIA), which introduces a new neural network that serves as a feedback control to learn the minimizer; see [1] in the direct approach, and [2; 20; 22; 37] in the SDE-based approach.

In this work, we aim to develop a new deep learning method for very high-dimensional parabolic PDEs and stochastic optimal control problems (SOCs). To combine the advantages of the direct approach and the SDE-based approach, our method consists of the following techniques:

1. Following the idea of DeepMartNet [5; 7], we introduce the system process to cast the parabolic PDE into a martingale formulation, which avoids computing all kinds of derivatives in the original problem.
2. The martingale formulation is carefully designed for quasilinear PDEs such that, the sample path for exploring space can be simulated in an offline manner prior to training, and the martingale property is enforced on a series of system processes simulated in parallel across time, enabling mini-batch sampling and parallel computation of the loss function across both spatial and temporal directions.
3. Following the approach of SOC-MartNet proposed in [6], we enforce the martingale formulation using the Galerkin method combined with adversarial learning

techniques. This avoids computing the conditional expectations individually for each sampled state, and dramatically reduces the computational cost.

4. For the HJB equations and the associated SOCPs, we integrate the martingale formulation into the framework of PIA, such that the value function and the optimal feedback control can be solved simultaneously in a derivative-free manner without pointwise minimization.

By integrating these techniques, we arrive at a martingale deep learning method for PDEs and SOCPs. Numerical results demonstrate that our method can efficiently solve the HJB equation without explicit optimal control in dimensions upto 10^4

The rest of this paper is organized as follows. In section 2, the martingale deep learning method is proposed to solve quasilinear parabolic PDEs. In section 3, the proposed method is extended to solve HJB equations. Section 4 presents the numerical results. Some concluding remarks are given in section 5.

2 Martingale deep learning for quasilinear PDEs

We consider a class of quasilinear parabolic PDEs as

$$(\partial_t + \mathcal{L})v(t, x) + f(t, x, v(t, x)) = 0, \quad (t, x) \in [0, T] \times \mathbb{R}^d \quad (1)$$

with a specific terminal condition $v(T, x) = g(x)$ for $x \in \mathbb{R}^d$. Here \mathcal{L} is the differential operator as

$$\mathcal{L} := \mu^\top(t, x, v(t, x))\partial_x + \frac{1}{2} \text{Tr} \left\{ \sigma\sigma^\top(t, x, v(t, x)) \partial_{xx}^2 \right\} \quad (2)$$

for given functions μ and σ valued in \mathbb{R}^d and $\mathbb{R}^{d \times q}$, respectively. The operators $\partial_x = \nabla_x$ and $\partial_{xx}^2 = \nabla_x \nabla_x^\top$ are the gradient and Hessian operator, respectively, and Tr denotes the trace of a matrix. For a concise presentation of the main idea, the functions μ , σ and v are assumed to be smooth enough to validate the involved truncation error estimates.

2.1 Martingale formulation

To present the martingale formulation of Eq. (1), we shall extend the idea of DeepMartNet proposed in [5; 7].

Let $(\Omega, \mathcal{F}, \mathbb{F}, \mathbb{P})$ be a filtered complete probability space with $\mathbb{F} := (\mathcal{F}_t)_{0 \leq t \leq T}$ the natural filtration of the standard q -dimensional Brownian motion $B : [0, T] \times \Omega \rightarrow \mathbb{R}^q$. We introduce a pilot process $\hat{X} : [0, T] \times \Omega \rightarrow \mathbb{R}^d$ used to explore space \mathbb{R}^d . A typical example of \hat{X} can be given by the SDE

$$\hat{X}_t = \hat{X}_0 + \int_0^t \hat{\mu}(s, \hat{X}_s) ds + \int_{t_n}^t \hat{\sigma}(s, \hat{X}_s) dB_s \quad (3)$$

for $t \in [0, T]$, where $\hat{\mu}(t, x) := \mu(t, x, \hat{v}(t, x))$ and $\hat{\sigma}(t, x) := \sigma(t, x, \hat{v}(t, x))$ for $(t, x) \in [0, T] \times \mathbb{R}^d$ with \hat{v} an initial guess of v , and the stochastic integral with respect to B_s is of Itô type. For $0 \leq s \leq t \leq T$, let $t \mapsto X_t^s$ be the system process starting from \hat{X}_s and generated by the operator \mathcal{L} , that is,

$$X_t^s = \hat{X}_s + \int_s^t \mu(r, X_r^s, v(r, X_r^s)) dr + \int_s^t \sigma(r, X_r^s, v(r, X_r^s)) dB_r, \quad (4)$$

and the superscript s indicates that the system process X_t^s starts at the time s .

We are ready to introduce the martingale formulation based on the system process

X_t^s . For any smooth $v \in C^{1,2}$, we apply the Itô formula to $t \mapsto v(t, X_t^s)$, yielding that

$$v(t, X_t^s) - v(s, X_s^s) = \int_s^t (\partial_t + \mathcal{L})v(r, X_r^s) dr + \int_s^t (\partial_x v)^\top \sigma(r, X_r^s, v(r, X_r^s)) dB_r,$$

which further implies

$$\mathcal{M}_t^s := v(t, X_t^s) - v(s, X_s^s) + \int_s^t f(r, X_r^s, v(r, X_r^s)) dr \quad (5)$$

$$= \int_s^t R(r, X_r^s; v) dr + \int_s^t (\partial_x v)^\top \sigma(r, X_r^s) dB_r, \quad (6)$$

where $R(t, x; v)$ denotes the residual error of the PDE in Eq. (1) of the function $v(t, x)$, i.e.,

$$R(t, x; v) := (\partial_t + \mathcal{L})v(t, x) + f(t, x, v(t, x)). \quad (7)$$

Under some usual conditions, the system process $\{X_t^s : t \in [s, T]\}$ is Markovian relative to the filtration \mathbb{F} [31, Definition 17.2.1, Theorem 17.2.3]. Moreover, the Itô integral in Eq. (6) is an \mathbb{F} -martingale for $t \in [s, T]$ [27, Corollary 3.2.6], and thus it can be canceled by taking the conditional expectation $\mathbb{E}[\cdot | X_s^s]$, yielding that

$$\mathbb{E}[\mathcal{M}_t^s | X_s^s] = \int_s^t \mathbb{E}[R(r, X_r^s; v) | X_s^s] dr, \quad t \in [s, T]. \quad (8)$$

Letting t approach s and noticing that $X_s^s = \hat{X}_s$, we can recover the residual error R from Eq. (8) by

$$\mathbb{E}[\mathcal{M}_{s+h}^s | \hat{X}_s] = hR(s, \hat{X}_s; v) + O(h^2), \quad 0 \leq s \leq T - h \quad (9)$$

under sufficient regularity conditions, where $h > 0$ is a small time step size. Eq. (7) and Eq. (9) suggest that we can solve the PDE in Eq. (1) by finding v such that \mathcal{M}_t^s fulfill a martingale property around $t \rightarrow s+$. Then we propose the martingale formulation for Eq. (1):

$$\mathbb{E}[\mathcal{M}_{t+h}^t | \hat{X}_t] = 0, \quad 0 \leq t \leq T - h. \quad (10)$$

Our martingale formulation in Eq. (10) is originated from the DeepMartNet [5; 7]. In the DeepMartNet, the martingale formulation is enforced on the paths of $t \mapsto X_t^0$ given by Eq. (4) over the entire time interval $t \in [0, T]$. However, in Eq. (10), the entire diffusion $t \mapsto X_t^0$ is replaced by a series of system processes $s \mapsto X_s^t$ on the small time intervals $s \in [t, t+h]$.

This change yields the following features compared with existing works:

- The DeepMartNet and other SDE-based approaches, such as [8; 13; 14; 15; 26; 30; 36], require the simulation of paths for $t \mapsto X_t^0$. This involves solving Eq. (4) with $s = 0$ over the entire time interval $t \in [0, T]$. Moreover, Eq. (4) relies on the unknown function v under approximation, which means that Eq. (4) needs to be re-computed whenever the approximation of v is updated. This re-computing process is sequential in time and imposes substantial computational costs.
- For the martingale formulation in Eq. (10), the simulations of the system processes $t+h \mapsto X_{t+h}^t$ are decoupled across the time steps $t \in [0, T-h]$. This enables mini-batch sampling of the time steps $t \in [0, T-h]$, allowing the martingale property in Eq. (10) to be enforced individually and in parallel for each sampled time step. This feature significantly speed up the computation of our method.

Remark 1. Recalling Eq. (9), we conclude that the martingale condition in Eq. (10) guarantees the residual error $R(t, \hat{X}_t; v)$ vanishes in the region explored by the pilot pro-

cess \hat{X}_t . Thus a reasonable pilot process should explore the regions of interest with a higher probability.

2.2 Martingale formulation combined with a Galerkin method

Compared with the original PDE in Eq. (1), the desirable feature of Eq. (10) is derivative-free, which constitute a fundamental improvement over the DeepMartNet and SOC-MartNet proposed in [5; 6; 7]. However, this feature comes at the cost of approximating the conditional expectation for samples of \hat{X}_t . To address this issue, we shall reformulate Eq. (10) into a weak form.

Let \mathcal{T} be the set of test functions consisting of all bounded and smooth function on $[0, T] \times \mathbb{R}^d$, then Eq. (10) can be ensured by

$$\int_0^{T-h} \mathbb{E}[\rho(t, \hat{X}_t) \mathbb{E}[\mathcal{M}_{t+h}^t | \hat{X}_t]] dt = 0 \quad (11)$$

for any $\rho \in \mathcal{T}$. Since $\rho(t, \hat{X}_t)$ is \hat{X}_t -measurable, it can be moved into $\mathbb{E}[\cdot | \hat{X}_t]$, yielding that

$$\begin{aligned} \mathbb{E}[\rho(t, \hat{X}_t) \mathbb{E}[\mathcal{M}_{t+h}^t | \hat{X}_t]] &= \mathbb{E}[\mathbb{E}[\rho(t, \hat{X}_t) \mathcal{M}_{t+h}^t | \hat{X}_t]] \\ &= \mathbb{E}[\rho(t, \hat{X}_t) \mathcal{M}_{t+h}^t] \\ &\approx \mathbb{E}[\rho(t, \hat{X}_t) \mathcal{M}(t, \hat{X}_t, \xi; v)] \end{aligned} \quad (12)$$

where $\mathcal{M}(t, \hat{X}_t, \xi; v)$ is a weak approximation of \mathcal{M}_{t+h}^t obtained by applying the Euler approximation to Eq. (4) and Eq. (5), namely

$$\mathcal{M}(t, x, w; v) := v(t+h, x + \mu(t, x)h + \sigma(t, x)\sqrt{hw}) - v(t, x) + hf(t, x, v(t, x)) \quad (13)$$

for $(t, x, w) \in [0, T] \times \mathbb{R}^d \times \mathbb{R}^q$ and $\xi \sim \mathcal{N}(0, I_q)$ with I_q the q -dimensional identity matrix.

Inserting Eq. (12) into Eq. (11), we obtain a martingale formulation free of conditional expectations:

$$\min_{v \in \mathcal{V}} \sup_{\rho \in \mathcal{T}} |G(v, \rho)|^2 = 0, \quad (14)$$

where $G(v, \rho)$ is the loss function defined by

$$G(v, \rho) := \int_0^{T-h} \mathbb{E}[\rho(t, \hat{X}_t) \mathcal{M}(t, \hat{X}_t, \xi; v)] dt, \quad (15)$$

and \mathcal{V} denotes the set of candidate solutions v satisfying the terminal condition, i.e.,

$$\mathcal{V} := \left\{ v \in C^{1,2} : v(T, x) = g(x), \quad x \in \mathbb{R}^d \right\}. \quad (16)$$

Remark 2. The approximation error of Eq. (12) is of order $O(h^2)$, following from the facts that the Euler scheme applied to Eq. (4) enjoys a local truncation error of weak-2nd order [23, Propostion 5.11.1] and the left-rectangular quadrature formula applied to the integral in Eq. (5) is of 2nd order, too.

2.3 Adversarial learning for the martingale formulation

The minimax problem in Eq. (14) can be naturally solved by adversarial learning as in [35].

Specifically, we approximate the functions v and ρ by neural networks v_θ and ρ_η parameterized by θ and η , respectively. To fulfill the terminal condition $v(T, x) = g(x)$

for $x \in \mathbb{R}^d$, the network v_θ takes the form of

$$v_\theta(t, x) := \begin{cases} \phi_\theta(t, x), & (t, x) \in [0, T] \times \mathbb{R}^d, \\ g(x), & (t, x) \in \{T\} \times \mathbb{R}^d, \end{cases} \quad (17)$$

where $\phi_\theta : [0, T] \times \mathbb{R}^d \rightarrow \mathbb{R}$ a neural network parameterized by θ .

The adversarial network ρ_η plays the role of test functions. By our experiment results, ρ_η is not necessarily to be very deep, but instead, it can be a shallow network with enough output dimensionality. Following the multiscale neural network approach in [24; 25], we consider a typical ρ_η in the form of

$$\rho_\eta(t, x) = \sin(\Lambda(W_1 t + W_2 x) + b) \in \mathbb{R}^r, \quad (18)$$

where $\eta := (W_1, W_2, b) \in \mathbb{R}^r \times \mathbb{R}^{r \times d} \times \mathbb{R}^r$ is the training parameter; $\Lambda(\cdot)$ is a scale layer defined by

$$\Lambda(y_1, y_2, \dots, y_r) = (c y_1, 2c y_2, \dots, r c y_r)^\top \in \mathbb{R}^r$$

for $y_1, y_2, \dots, y_r \in \mathbb{R}$ and $c > 0$ is a fixed hyper-parameter; $\sin(\cdot)$ is the activation function applied on the outputs of Λ in an element-wise manner.

The neural networks can be trained to fit Eq. (14) by stochastic gradient algorithms with the expectation in Eq. (15) approximated by mini-batch sampling. Specially, we introduce a uniform time partition on $[0, T]$, i.e., $t_n = nh$ for $n = 0, 1, \dots, N$ with the step size $h = T/N$. By applying the Euler scheme to Eq. (3), the sample paths of the pilot process \hat{X} are generated by

$$\hat{X}_{n+1}^m = \hat{X}_n^m + \hat{\mu}(t_n, \hat{X}_n^m)h + \hat{\sigma}(t_n, \hat{X}_n^m)\sqrt{h}\xi_n^m \quad (19)$$

for $n = 0, 1, \dots, N-1$ and $m = 1, 2, \dots, M$, where all ξ_n^m are i.i.d. samples from $N(0, I_q)$. Then we define the empirical version of G as

$$G(v, \rho; A) := \frac{h}{|A|} \sum_{(n,m) \in A} \rho(t_n, \hat{X}_n^m) \mathcal{M}(t_n, \hat{X}_n^m, \xi_n^m; v), \quad (20)$$

where \mathcal{M} is given in Eq. (13), and A is a index subset randomly taken from $\{0, 1, \dots, N-1\} \times \{1, 2, \dots, M\}$. Further, the loss function in Eq. (14) can be estimated by

$$|G(v, \rho)|^2 \approx G(v, \rho; A_1)G(v, \rho; A_2). \quad (21)$$

where A_1 and A_2 are random index subsets satisfying

$$A_1, A_2 \subset \{0, \dots, N-1\} \times \{1, \dots, M\}, \quad A_1 \cap A_2 = \emptyset. \quad (22)$$

Here, inspired by [12; 19], the sets A_1 and A_2 are disjoint to ensure the mini-batch estimation in Eq. (21) is unbiased.

Finally, the minimax problem in Eq. (14) can be solved by alternating gradient descent and ascent of $G(v_\theta, \rho_\eta; A_1)G(v_\theta, \rho_\eta; A_2)$ over θ and η , respectively. The details are presented in Algorithm 1.

In the following, we summarize the desirable features of the weak martingale formulation in Algorithm 1:

- **Derivative-free approach:** Different from the deep learning methods directly applied on Eq. (1), Algorithm 1 is free of computing any derivatives by automatic differentiation, especially the $d \times d$ -dimensional Hessian matrix $\partial_{xx}^2 v$, which generate much gain in efficiency for problems with very high spatial dimensionality.
- **Parallel loss computation:** The sample paths $\{\hat{X}_n^m\}_{n=0}^N$ are independent of any

Algorithm 1 Weak martingale formulation for PDEs

Input: I : the maximum number of iterations of stochastic gradient algorithm; M : the total number of sample paths for exploring \mathbb{R}^d ; δ_1/δ_2 : learning rate for the network v_θ/ρ_η ; J/K : number of θ/η updates per iteration.

- 1: Initialize the networks v_θ and ρ_η
 - 2: Generate the sample paths $\{(\hat{X}_n^m, \xi_n^m)\}_{n=0}^N$ by Eq. (19).
 - 3: **for** $i = 0, 1, \dots, I - 1$ **do**
 - 4: Sample disjoint index subsets A_1, A_2 per Eq. (22).
 - 5: **for** $j = 0, 1, \dots, J - 1$ **do**
 - 6: $\theta \leftarrow \theta - \delta_1 \nabla_\theta \{G(v_\theta, \rho_\eta; A_1)G(v_\theta, \rho_\eta; A_2)\}$
 - 7: **end for**
 - 8: **for** $k = 0, 1, \dots, K - 1$ **do**
 - 9: $\eta \leftarrow \eta + \delta_2 \nabla_\eta \{G(v_\theta, \rho_\eta; A_1)G(v_\theta, \rho_\eta; A_2)\}$
 - 10: **end for**
 - 11: **end for**
- Output:** v_θ
-

unknown quantity to be learned, and can be simulated offline using Eq. (19) prior to training. Throughout training, all the summation terms in Eq. (20) can be computed parallelly even in the time direction. This feature differs significantly from existing SDE model-based deep learning methods, whose sample paths typically need to be updated throughout training, in a sequential fashion over time.

3 Extension to HJB equations

Now we shall extend the martingale deep learning method to solve the HJB equation in the form of

$$\partial_t v(t, x) + \inf_{\kappa \in U} \{\mathcal{L}^\kappa v(t, x) + c(t, x, \kappa)\} = 0 \quad (23)$$

for $(t, x) \in [0, T] \times \mathbb{R}^d$ with a terminal condition the same as Eq. (1), where \mathcal{L}^κ is an analogue of \mathcal{L} in Eq. (2) additionally controlled by $\kappa \in U \subset \mathbb{R}^m$ namely

$$\mathcal{L}^\kappa := \mu^\top(t, x, \kappa) \partial_x + \frac{1}{2} \text{Tr} \left\{ \sigma \sigma^\top(t, x, \kappa) \partial_{xx}^2 \right\} \quad (24)$$

for $(t, x, \kappa) \in [0, T] \times \mathbb{R}^d \times U$, and μ, σ and c are all given functions valued in $\mathbb{R}^d, \mathbb{R}^{d \times q}$ and \mathbb{R} , respectively.

3.1 Policy improvement algorithm (PIA)

Compared to Eq. (1), the HJB equation in Eq. (23) is more challenging due to its optimization component $\inf_{\kappa \in U} \{\dots\}$. This infimum is generally implicit without a closed-form expression, and direct applying conventional PDE solvers to Eq. (23) involves computing $\inf_{\kappa \in U}$ for each (t, x) , resulting in a CoD computation cost. To overcome this difficulty, we follow the idea of PIA considered in [1], and decompose Eq. (23) into two stages

$$(\partial_t + \mathcal{L}^u)v(t, x) + c(t, x, u(t, x)) = 0, \quad (25)$$

$$u(t, x) = \arg \min_{\kappa \in U} \{\mathcal{L}^\kappa v(t, x) + c(t, x, \kappa)\}, \quad (26)$$

for $(t, x) \in [0, T] \times \mathbb{R}^d$, with $\mathcal{L}^u := \mathcal{L}^{u(t, x)}$. In the context of SOCPs, the functions u and v are just the optimal feedback control and the value function, respectively; see, e.g., [28; 34].

In the following, we shall extend the martingale deep learning method for Eq. (25) and Eq. (26) to obtain a numerical solution for both the value function and the optimal control simultaneously.

3.2 Martingale formulation for the value function

Given u , Eq. (25) degenerates into a linear PDE, which can be directly solved by the method introduced in the last section. Thus, mimicking Eq. (14), the value function v is solved by

$$\min_{v \in \mathcal{V}} \sup_{\rho \in \mathcal{T}} |G(u, v, \rho)|^2, \quad (27)$$

where, by slight abuse of notation, G is defined by

$$G(u, v, \rho) := \int_0^{T-h} \mathbb{E} \left[\rho(t, \hat{X}_t) \mathcal{M} \left(t, \hat{X}_t, \xi; u, v \right) \right] dt \quad (28)$$

with \hat{X} the pilot process exploring \mathbb{R}^d , $\xi \sim \mathcal{N}(0, I_q)$ and

$$\begin{aligned} \mathcal{M}(t, x, w; u, v) := & v \left(t+h, x + \mu(t, x, u(t, x))h + \sigma(t, x, u(t, x))\sqrt{h}w \right) \\ & - v(t, x) + hc(t, x, u(t, x)). \end{aligned} \quad (29)$$

For the HJB Eq. (23), a typical example of the pilot process \hat{X} can be given by Eq. (3) with $\hat{\mu}(t, x) = \mu(t, x, \hat{u}(t, x))$ and $\hat{\sigma}(t, x) = \sigma(t, x, \hat{u}(t, x))$, where \hat{u} is an initial guess of the optimal control function u given by Eq. (26).

Remark 3. *Similar to Eq. (14) for quasilinear PDEs, a desirable feature of Eq. (27) is that the process X_t is independent of the unknown control u . This allows for the offline simulation of sample paths prior to training, eliminating the need for re-simulation whenever u is updated. Additionally, this feature enables parallel computation and mini-batch sampling for the loss function G in Eq. (28) across time steps.*

3.3 Martingale formulation for the optimal control

To propose a derivative-free approach for the optimal control, we shall present a martingale formulation for Eq. (26). First, to avoid pointwise minimization problem for each (t, x) , we follow the approach suggested by [1] and recast Eq. (26) into an equivalent integral version as

$$\min_{u \in \mathcal{U}_{\text{ad}}} \int_0^T \mathbb{E} \left[\mathcal{L}^u v(t, \hat{X}_t) + c \left(t, \hat{X}_t, u(t, \hat{X}_t) \right) \right] dt, \quad (30)$$

where \mathcal{U}_{ad} denotes the set of admissible feedback controls defined by

$$\mathcal{U}_{\text{ad}} := \left\{ u : [0, T] \times \mathbb{R}^d \rightarrow U \mid u \text{ is Borel measurable} \right\}. \quad (31)$$

We remark that $u(t, x)$ is a function of (t, x) , and thus Eq. (30) ensures $u(t, x)$ minimizes $\mathcal{L}^u v(t, x) + c(t, x, \kappa)$ pointwisely for each (t, x) explored by \hat{X}_t .

To eliminate the derivatives in Eq. (30), inserting Eq. (7) into Eq. (9), and further comparing Eq. (5) and Eq. (29), we can obtain

$$\mathbb{E} \left[\mathcal{M} \left(t, \hat{X}_t, \xi; u, v \right) \right] = h \left\{ (\partial_t + \mathcal{L}^u) v(t, \hat{X}_t) + c(t, \hat{X}_t, u(t, \hat{X}_t)) \right\} + O(h^2)$$

with the reminder term holding for sufficient regularity conditions. Inserting the above

equality into Eq. (30), and omitting the reminder term, we obtain

$$\min_{u \in \mathcal{U}_{\text{ad}}} \int_0^{T-h} h^{-1} \mathbb{E} \left[\mathcal{M} \left(t, \hat{X}_t, \xi; u, v \right) - \partial_t v(t, \hat{X}_t) \right] dt.$$

Since h^{-1} and $\partial_t v(t, \hat{X}_t)$ do not affect the minimizer, they can be dropped. This leads to the martingale formulation for the optimal control:

$$\min_{u \in \mathcal{U}_{\text{ad}}} G(u, v, 1) \quad (32)$$

with $G(u, v, 1)$ defined in Eq. (28).

3.4 Adversarial learning for value/control functions

The value function v and the optimal control u of Eq. (23) can be solved by training neural networks to satisfy Eq. (27) and Eq. (32), simultaneously. Specifically, similar to the last section, the functions (u, v, ρ) are approximated by neural networks $(u_\alpha, v_\theta, \rho_\eta)$ parameterized by α, θ and η , respectively, where v_θ and ρ_η still take the form of Eq. (17) and Eq. (18).

For the control network u_α , its range should be restricted in the control space U . If $U = [a, b] := \prod_{i=1}^m [a_i, b_i]$ with a_i, b_i the i -th elements of $a, b \in \mathbb{R}^m$, the structure of u_α can be

$$u_\alpha(t, x) = a + \frac{b-a}{6} \text{ReLU6}(\psi_\alpha(t, x)), \quad (33)$$

where $\text{ReLU6}(y) := \min\{\max\{0, y\}, 6\}$ is an activation function and $\psi_\alpha : [0, T] \times \mathbb{R}^d \rightarrow \mathbb{R}^m$ is a neural network with parameter α . Remark 4 provides a penalty method to deal with general control spaces.

To satisfy Eq. (27) and Eq. (32) simultaneously, the neural networks v_θ, u_α and ρ_η can be trained alternately by

1. minimizing $|G(u_\alpha, v_\theta, \rho_\eta)|^2$ over θ ;
2. maximizing $|G(u_\alpha, v_\theta, \rho_\eta)|^2$ over η ;
3. minimizing $|G(u_\alpha, v_\theta, 1)|$ over α .

Similar to the last section, the above training procedure can be implemented by stochastic gradient algorithms with G replaced by its mini-batch version:

$$G(u, v, \rho; A_i) := \frac{h}{|A_i|} \sum_{(n,m) \in A_i} \rho(t_n, \hat{X}_n^m) \mathcal{M} \left(t_n, \hat{X}_n^m, \xi_n^m; u, v \right), \quad (34)$$

where (\hat{X}_n^m, ξ_n^m) are samples of \hat{X}_{t_n} and $\xi \sim \mathcal{N}(0, I_q)$, and $A_i, i = 1, 2$, are given in Eq. (22); \mathcal{M} is given in Eq. (29). The detailed training algorithm is presented in Algorithm 2.

Remark 4. *If the control space U is general rather than an interval, the network structure in Eq. (33) is no longer applicable. This issue can be addressed by appending a new penalty term $\bar{\lambda} \int_0^T \mathbb{E} \left[\text{dist} \left(u_\alpha(t, \hat{X}_t), U \right) \right] dt$ on the right side of Eq. (32) to ensure $u_\alpha(t, \hat{X}_t)$ remains within U , where $\bar{\lambda} \geq 0$ is a penalty coefficient and $\text{dist}(\kappa, U)$ denotes a certain distance between $\kappa \in \mathbb{R}^m$ and U .*

Remark 5. *Compared with the original SOC-MartNet proposed in [6], the derivative-free version in Algorithm 2 enjoys the following features:*

- *The loss function Eq. (34) is free of computing $\partial_x v$ and $\partial_{xx}^2 v$, where the latter is quite expensive for high-dimensional problems.*

Algorithm 2 Derivative-free SOC-MartNet for solving the HJB Eq. (23)

Input: I : the maximum number of iterations of stochastic gradient algorithm; M : the total number of sample paths for exploring \mathbb{R}^d ; $\delta_1/\delta_2/\delta_3$: learning rate for the network $v_\theta/u_\alpha/\rho_\eta$; J/K : number of $(\theta, \alpha)/\eta$ updates per iteration.

```
1: Initialize the networks  $u_\alpha, v_\theta$  and  $\rho_\eta$ 
2: Generate the samples  $\{(\hat{X}_n^m, \xi_n^m)\}_{n=0}^N$  of  $\{(\hat{X}_{t_n}, \xi)\}_{n=0}^N$  for  $m = 1, 2, \dots, M$ .
3: for  $i = 0, 1, \dots, I - 1$  do
4:   Sample disjoint index subsets  $A_1, A_2$  per Eq. (22).
5:   for  $j = 0, 1, \dots, J - 1$  do
6:      $\theta \leftarrow \theta - \delta_1 \nabla_\theta \{G(u_\alpha, v_\theta, \rho_\eta; A_1)G(u_\alpha, v_\theta, \rho_\eta; A_2)\}$ 
7:      $\alpha \leftarrow \alpha - \delta_2 \nabla_\alpha G(u_\alpha, v_\theta, 1; A_1 \cup A_2)$ 
8:   end for
9:   for  $k = 0, 1, \dots, K - 1$  do
10:     $\eta \leftarrow \eta + \delta_3 \nabla_\eta \{G(u_\alpha, v_\theta, \rho_\eta; A_1)G(u_\alpha, v_\theta, \rho_\eta; A_2)\}$ 
11:  end for
12: end for
Output:  $u_\alpha$  and  $v_\theta$ 
```

- However, the random jumps $\xi_h^{t,x} := \mu(t, x, u(t, x))h + \sigma(t, x, u(t, x))\sqrt{h}\xi$ in Eq. (29) depends on the optimal control u under approximation, therefore need to be updated along with the optimal control. This implies those jumps can not be pre-calculated before the training as in the original SOC-MartNet.

4 Numerical Examples

We will demonstrate the effectiveness of our method by applying Algorithms 1 and 2 to a series of benchmark problems. In these tests, both networks u_α and v_θ are fully-connected with 4 hidden layers. The number of hidden units per layer, denoted as W , will be reported in the numerical results. When presenting these results, the abbreviations “RE”, “SD”, “RT” and “vs” are used for “relative error”, “standard deviation”, “runtime” and “versus”, respectively. Additional detailed parameter settings are provided in the appendix.

4.1 Allen-Cahn equations

We consider the following Allen-Cahn equation from [13]:

$$\frac{\partial v}{\partial t}(t, x) + \Delta_x v(t, x) + v(t, x) - \{v(t, x)\}^3 = 0 \quad (35)$$

for $(t, x) \in [0, T) \times \mathbb{R}^d$ with the terminal condition $v(T, x) = 1/(2 + 0.4|x|^2)$ for $x \in \mathbb{R}^d$. Following the setting of [13], we set $T = 0.3$, $d = 100$, and solve $v(0, x_0)$ at $x_0 = (0, \dots, 0)^\top \in \mathbb{R}^{100}$. The reference solution is $v(0, x_0) \approx 0.0528$ according to [13] obtained by the branching diffusion method [17; 18]. By applying Algorithm 1 to Eq. (35), the relevant numerical results are depicted in Figure 1. The curve in Figure 1 demonstrates the efficiency of our method, which successfully solves a 100-dimensional problem while achieving a relative error of 0.32% within a runtime of just 6.8 seconds.

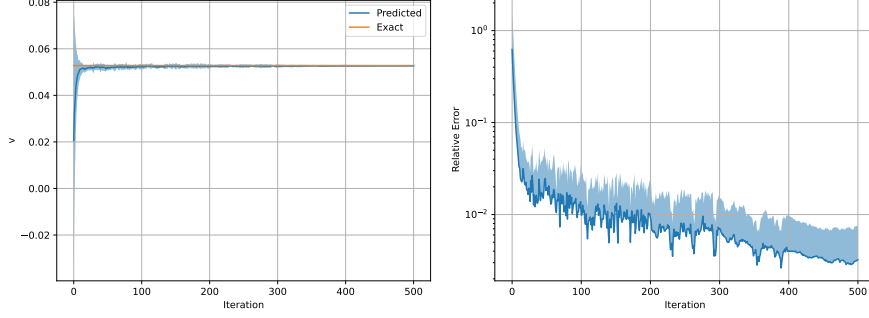


Figure 1 Numerical results of Algorithm 1 applied to the Allen-Cahn equation Eq. (35) with $d = 100$. (Left) The reference and predicted values of $v(0, x_0)$ versus the iteration steps with $x_0 = (0, \dots, 0)^\top \in \mathbb{R}^{100}$. The shaded region represents the mean $\pm 2 \times SD$ of v_θ across 10 independent runs. The widths of u_α and v_θ are both $W = 2d + 10$. (Right) RE of $v(0, x_0)$ vs iteration steps, where shaded region represents the mean $+2 \times SD$ of the RE across 10 independent runs. The mean RE and the SD achieve 3.2×10^{-3} and 2.1×10^{-3} , respectively, at the 500-th iteration step within a runtime less than 6.8 seconds.

4.2 Diffusion equations in high dimensionality

We now consider a problem with dimensionality up to 10^4 . To construct a PDE with a known exact solution, a source term is introduced to the left side of Eq. (35), yielding

$$\frac{\partial v}{\partial t}(t, x) + \Delta_x v(t, x) + v(t, x) - \{v(t, x)\}^3 + Q(t, x) = 0, \quad (36)$$

where the function $Q(t, x)$ and the terminal condition $v(T, x) = g(x)$ are chosen such that Eq. (36) admits an exact solution given by

$$v(t, x) = V((t - 0.5)\mathbf{1}_d + x), \quad (t, x) \in [0, T] \times \mathbb{R}^d, \quad (37)$$

where $\mathbf{1}_d := (1, 1, \dots, 1)^\top \in \mathbb{R}^d$, and V is a function modified from (28) in [19] and given by

$$V(x) := \sum_{i=1}^{d-1} c_i S(x_i, x_{i+1}) + c_d S(x_d, x_1) \quad (38)$$

with $c_i := (1.5 - \cos(i\pi/d))/d$ and

$$S(x_i, x_j) := \sin(x_i + \cos(x_j) + x_j \cos(x_i)). \quad (39)$$

Similar to the discussions in [19], the function $V(x)$ defined in Eq. (38) incorporates uneven coefficients c_i and pairwise interactions between the variables x_i and x_{i+1} . These factors complicate the structure of the problem, making the exact solution $v(t, x)$ in Eq. (37) highly nontrivial and challenging.

To better illustrate the behaviors of Algorithm 1, we apply it to Eq. (36) with $d = 10^4$ under three parameter settings:

1. Setting 1: Algorithm 1 solves $v(0, x)$ at a single spatial point $x = -0.5\mathbf{1}_d$. All pilot paths \hat{X} , defined in Eq. (3), start at the fixed point $\hat{X}_0 = -0.5\mathbf{1}_d$. The width W of v_θ is set to 1024, which is far smaller than $d = 10^4$, and results in limited expressive capacity.
2. Setting 2: Algorithm 1 solves $v(0, x)$ for x lying along the line segment $D_0 := \{s\mathbf{1}_d : s \in S\}$ with $S := [-1.5, 1.5]$. The segment D_0 has length $3\sqrt{d}$, making the problem increasingly challenging as d grows. The starting points \hat{X}_0 of the pilot paths are uniformly sampled from D_0 . The network width remains fixed at $W = 1024$.

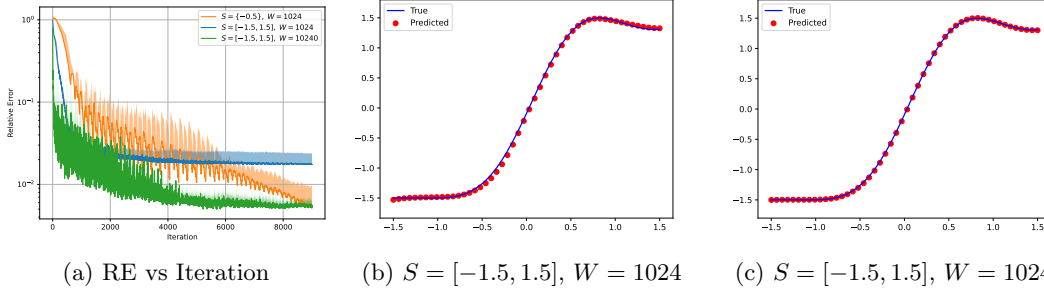


Figure 2 Numerical results of Algorithm 1 for Eq. (36) with $d = 10^4$. (Left) RE vs Iteration of Algorithm 1 in solving $v(0, s\mathbf{1}_d)$ for $s \in S$, under different combinations of S and W , where W is the width of v_θ . The shaded region represents the mean $+2 \times SD$ of the RE across 5 independent runs. The mean and the SD of RE, and the RT at the 9000-th iteration step are given in Table 1. (Middle and Right) The true and predicted values of $s \mapsto v(0, s\mathbf{1}_d)$ at the 9000-th iteration step under Settings 2 and 3.

Table 1 Numerical results of Algorithm 1 for Eq. (36) with $d = 10^4$. The algorithm solves $v(0, s\mathbf{1}_d)$ for $s \in S$ with the number of iteration steps set to 9000. The notation W denotes the network width of v_θ . More results are presented in Figure 2.

Setting	S	W	Mean of RE	SD of RE	RT (s)
1	$\{-0.5\}$	1024	5.5×10^{-3}	2.0×10^{-3}	295
2	$[-1.5, 1.5]$	1024	1.8×10^{-2}	3.1×10^{-3}	296
3	$[-1.5, 1.5]$	10240	5.4×10^{-3}	5.3×10^{-4}	5410

- Setting 3: the network width W is increased to 10240, allowing greater expressive power for v_θ . Other aspects are identical to Setting 2.

The relevant numerical results are presented in Figure 2 and Table 1. The following observations can be made:

- Algorithm 1 yields accurate solutions across all three parameter settings, as shown in Figure 2. Even in the case with the largest relative error (Figure 2(b)), the numerical solution still fit the exact solution well.
- Comparing Settings 1 and 2 in Table 1, the RE increases when the set S is expanded from $\{-0.5\}$ to $[-1.5, 1.5]$. The results for Setting 3 show that increasing the network width W from 1024 to 10240 mitigates this error. This suggests that the network’s expressive capacity can limit accuracy, particularly when the solution domain extends beyond a single point.
- Comparing Settings 2 and 3 in Table 1, increasing the network width W improves RE but also significantly increases the RT. This indicates a performance bottleneck caused by network expressivity when solving problems with dimensionality up to 10^4 . This bottleneck is likely shared by other deep learning methods relying on conventional neural network architectures.

4.3 Quasilinear parabolic PDEs

We turn to illustrate the performance of Algorithm 1 in solving PDEs with higher nonlinearity. Specially, the following quasilinear parabolic (QLP) equations with $d = 10^4$ are considered:

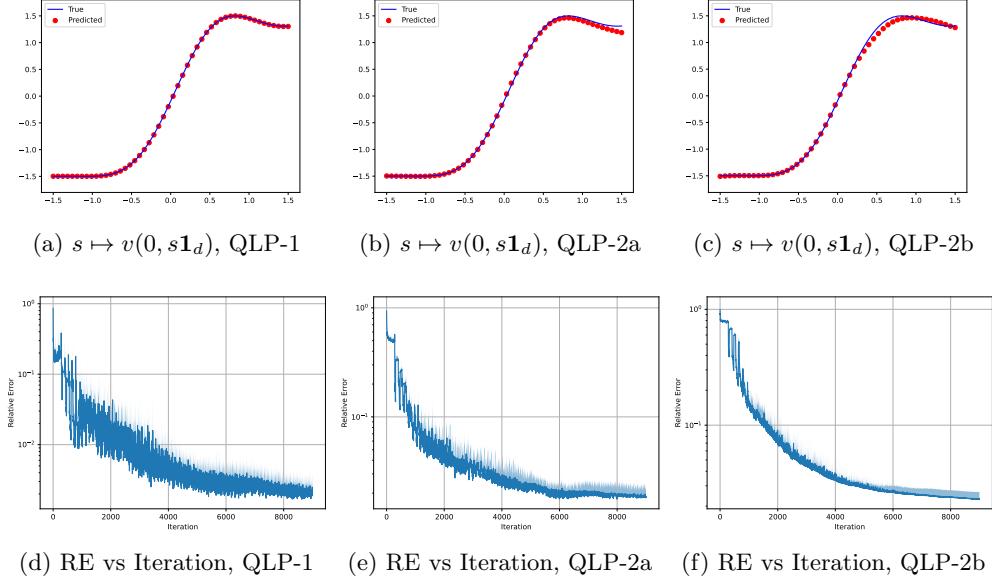


Figure 3 Numerical results of Algorithm 1 for $s \mapsto v(0, s\mathbf{1}_d)$ from various quasilinear PDEs with $d = 10^4$. The width of v_θ is set to $W = d + 10$. The shaded region represents the mean $+2 \times$ SD of the relative errors across 5 independent runs. The running times for each run are all less than 5500 seconds.

- QLP-1: it is given by Eq. (1) with a nonlinear diffusion term and Allen-Cahn-typed source term, i.e.,

$$\mathcal{L} = \frac{v^2}{2} \sum_{i=1}^d \partial_{x_i}^2, \quad f(t, x, v) = v - v^3 + Q(t, x); \quad (40)$$

- QLP-2a: it is given by Eq. (1) including nonlinearity in the drift, diffusion and source terms, i.e.,

$$\mathcal{L} = \left(\frac{v}{2} - 1\right) \sum_{i=1}^d \partial_{x_i} + \frac{v^2}{2} \sum_{i=1}^d \partial_{x_i}^2, \quad f(t, x, v) = v^2 + Q(t, x). \quad (41)$$

- QLP-2b: it is a more complex version of QLP-2a by replacing the diagonal diffusion coefficient with a dense one:

$$\mathcal{L} = \left(\frac{v}{2} - 1\right) \sum_{i=1}^d \partial_{x_i} + \frac{1}{2d^2} \sum_{i,j,k=1}^d \sigma_{ik} \sigma_{jk} \partial_{x_i} \partial_{x_j}, \quad f(t, x, v) = v^2 + Q(t, x), \quad (42)$$

$$\sigma_{ij} = \cos(x_i) + v \sin(x_j), \quad i, j = 1, 2, \dots, d.$$

In the above equations, the functions $Q(t, x)$ and the terminal conditions $v(T, x) = g(x)$ are chosen such that the PDE admits an exact solution given by Eq. (37). The relevant numerical results of Algorithm 1 are presented in Figure 3, where we can see that our method is effective and efficient in solving all the involved quasilinear equations for d upto 10^4 .

4.4 HJB equations

The numerical test is performed by applying Algorithm 2 to the HJB Eq. (23) with

$$\mathcal{L}^\kappa = (b + 2\kappa)^\top \partial_x + \delta^2 \text{Tr} \{ \partial_{xx}^2 \}, \quad c(t, x, \kappa) = \delta^{-2} |\kappa|^2, \quad U = \mathbb{R}^d, \quad T = 1, \quad (43)$$

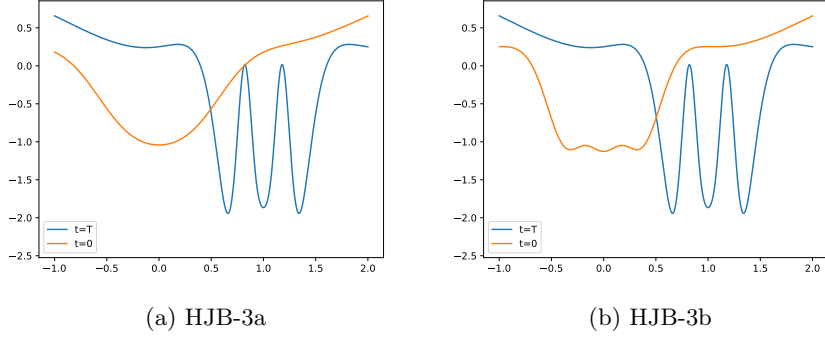


Figure 4 Graphs of the true solutions of HJB-3a and HJB-3b. The orange and the blue curves depict the mappings $s \mapsto v(0, s\mathbf{1}_d)$ and $s \mapsto v(T, s\mathbf{1}_d)$, respectively.

where $\delta > 0$, $b \in \mathbb{R}^d$ and the terminal condition $v(T, x) = g(x)$ will be specified later. By the Itô formula, the resulted HJB Eq. (23) admits an analytic solution given by

$$v(t, x) = -\ln \left(\mathbb{E} \left[\exp \left(-g(X_T^{t,x}) \right) \right] \right), \quad (44)$$

where

$$X_T^{t,x} = x + (T - t)b + \sqrt{2\delta}B_{T-t}, \quad B_{T-t} \sim N(0, I_d). \quad (45)$$

For a reference solution, the expectation in Eq. (44) is approximated by the Monte-Carlo method using 10^6 i.i.d. samples of $X_T^{t,x}$.

We consider the following specific HJB equations, which are the HJB given by Eq. (23) and Eq. (43) with different parameters:

- HJB-1: $b = 0$, $\delta = 1$, $v(T, x) = \ln(0.5(1 + |x|^2))$.
- HJB-2a: an variant of HJB-1 with $b = \mathbf{1}_d$ and $\delta = 0.1$.
- HJB-2b: an variant of HJB-2a with $\delta = 0.05$.
- HJB-3a: $b = \mathbf{1}_d$, $\delta = 0.2$, and $v(T, x) = \bar{g}(x - \mathbf{1}_d)$ with

$$\bar{g}(x) := \frac{1}{d} \sum_{i=1}^d \left\{ \sin(x_i - \frac{\pi}{2}) + \sin((0.1\pi + x_i^2)^{-1}) \right\}$$

- HJB-3b: an variant of HJB-3a with $\delta = 0.1$.

We have the following comments for the above equations: HJB-1 is a benchmark problem commonly used in existing works, such as [2; 8; 13; 16; 19; 22; 30; 33]. HJB-2a and -2b are modifications of HJB-1, featuring nonzero drift coefficients b and smaller diffusion coefficients δ in Eq. (45). These modifications result in a solution v that is less smooth compared to HJB-1. HJB-3a and -3b are more challenging than the previous equations due to their terminal function $\bar{g}(x)$, which is highly oscillatory around $x = 0$, resulting in a uneven solution when δ is small; see Figure 4 (a) and (b).

By applying Algorithm 2 to the above HJB equations, the relevant numerical results are presented in Figures 5 to 7. We have the following findings from the presented numerical results:

1. Figures 5 and 6 demonstrates the effectiveness of Algorithm 2 for solving high-dimensional problems with complex solution landscapes. The numerical solutions accurately approximate the true solution for HJB-3a, and capture the oscillatory outline of HJB-3b for $d = 2000$.

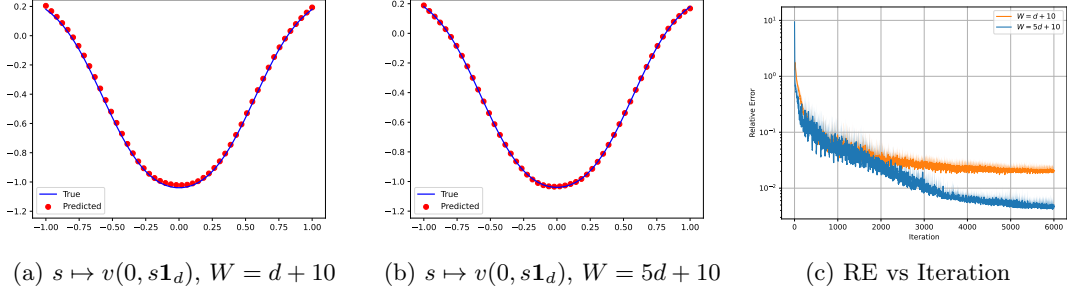


Figure 5 Numerical results of Algorithm 2 for HJB-3a with $d = 2000$. The subfigures (a) and (b) show the curves of $s \mapsto v(0, s\mathbf{1}_d)$ for $W = d + 10$ and $5d + 10$, respectively, where W denotes the widths of u_α and v_θ . The shaded region in (c) represents the mean $+2\times$ the SD of the RE across 5 independent runs. At the 6000-th iteration step, for $W = d + 10$, the mean and the SD of RE, and the RT are 2.1×10^{-2} , 1.7×10^{-3} and 540s, respectively; for $W = 5d + 10$, the corresponding values are 5.0×10^{-3} , 6.7×10^{-4} and 9050s.

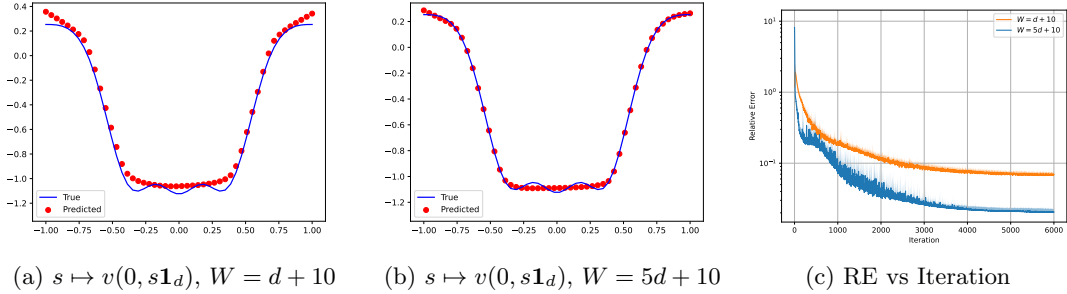


Figure 6 Numerical results of Algorithm 2 from HJB-3b with $d = 2000$. The subfigures (a) and (b) show the curves of $s \mapsto v(0, s\mathbf{1}_d)$ for $W = d + 10$ and $5d + 10$, respectively, where W denotes the widths of u_α and v_θ . The shaded region in (c) represents the mean $+2\times$ the SD of the RE across 5 independent runs. At the 6000-th iteration step, for $W = d + 10$, the mean and the SD of RE, and the RT are 6.9×10^{-2} , 3.6×10^{-3} , 540s, respectively; for $W = 5d + 10$, the corresponding values are 2.0×10^{-2} , 1.2×10^{-3} and 9050s.

- The REs in Figure 5(c) and Figure 6(c) show the impact of network width W of u_α and v_θ on the performance of Algorithm 2. Increasing W accelerates the error convergence for a fixed number of iterations. However, this comes at the cost of significantly increased computational time. Therefore, for large-scale problems with complex solutions, the performance of Algorithm 2 is likely bottlenecked by the limited capacity of small networks to represent high-dimensional functions.
- Figure 7 aims to demonstrate the capability of Algorithm 2 for solving extremely high-dimensional HJB equations. The numerical results show that no matter the solution is smooth or oscillatory, our method achieves satisfactory accuracy for $d = 10000$ within a running time of less than 9500 seconds.

5 Conclusions

In this work, a derivative-free martingale deep learning method is proposed for solving very high dimensional quasilinear parabolic PDEs and HJB equations. The method contains three key components: i) Reformulating the PDE and HJB equation into a martingale formulation. This reformulation avoids calculating any derivatives in the equations and allows for parallel computation across all random sampled time-states. ii) Enforcing the martingale formulation using the Galerkin method and adversarial learning

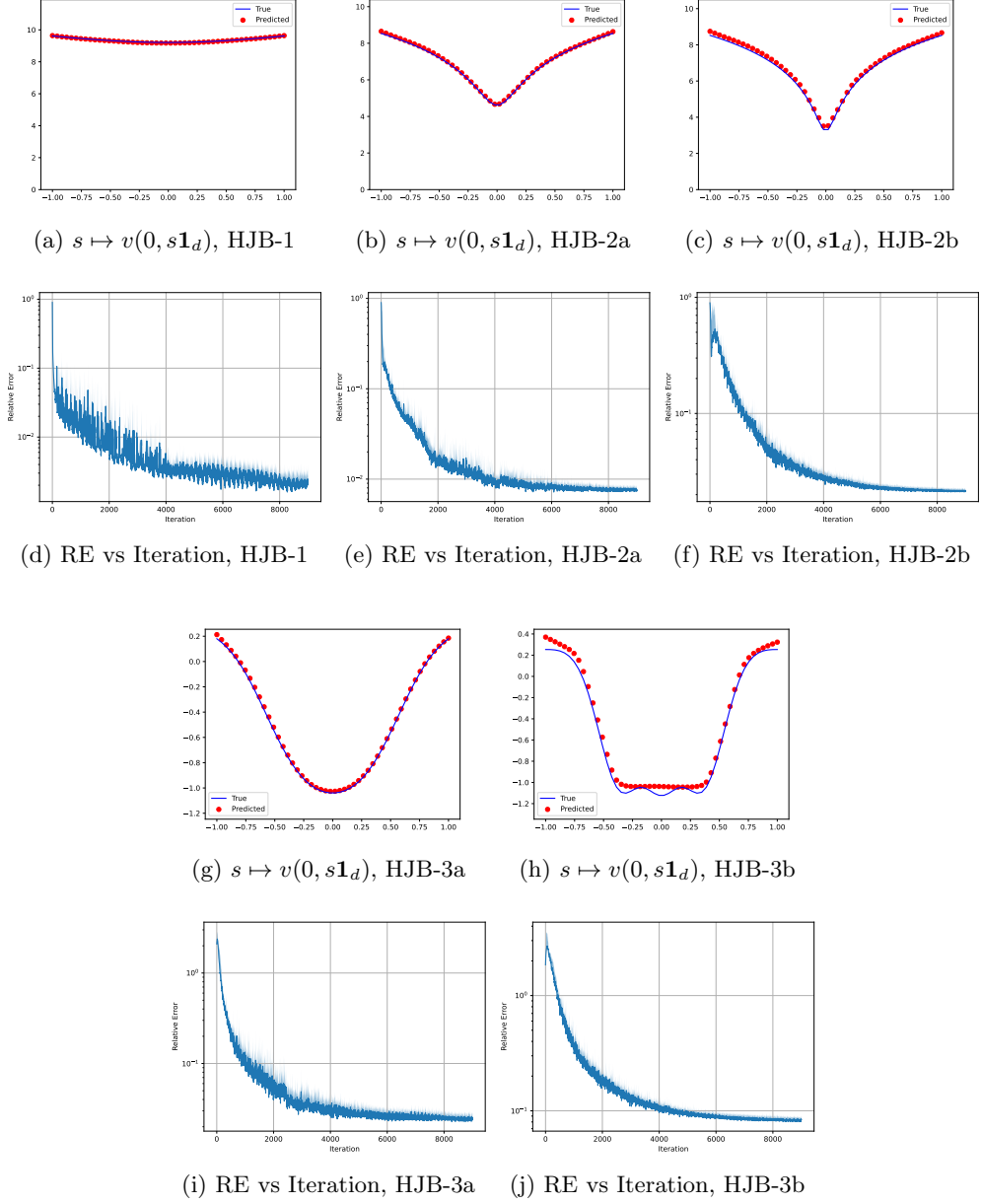


Figure 7 Numerical results of Algorithm 2 for $s \mapsto v(0, s\mathbf{1}_d)$ from various HJB equations with $d = 10^4$. The widths of u_α and v_θ are set to $W = d + 10$. The shaded region represents the mean $+2 \times$ the SD of the relative errors across 5 independent runs. The running times for each run are all less than 9500 seconds.

techniques, which avoids the need to compute conditional expectations for each time-state (t, x) . iii) Incorporating a PIA framework to the martingale formulation, which enables solving HJB equations without explicit optimal control. Our numerical results demonstrate that the proposed method is capable of accurately and efficiently solving HJB equations with complex solution landscapes and extremely high dimensionality (upto $d = 10^4$).

Appendix: Parameter settings for numerical tests

If no otherwise specified, the numerical methods solve $v(0, x)$ for $x \in D_0$, where D_0 is a spatial line segment defined by $D_0 := \{s\mathbf{1}_d : s \in [-r, r]\}$ with $r := 1$ and 1.5 for Eq. (1) and Eq. (23), respectively. For an approximation \hat{v} of v , its relative error $R(\hat{v})$ is given by

$$R(v_\theta) := \frac{\sum_{x \in D_0} |v_\theta(0, x) - v(0, x)|}{\sum_{x \in D_0} |v(0, x)|}.$$

In Algorithms 1 and 2, for each epoch, the sample paths \hat{X}_n^m of pilot processes are generated by

$$\hat{X}_{n+1}^m = \hat{X}_n^m + \mu \left(t_n, \hat{X}_n^m, u_n^m \right) \Delta t_n + \sigma \left(t_n, \hat{X}_n^m, u_n^m \right) \Delta B_{t_{n+1}}^m$$

for $m = 1, 2, \dots, M$ and $n = 0, 1, \dots, N - 1$, where $\Delta B_{t_{n+1}}^m := (B_{t_{n+1}}^m - B_{t_n}^m)$ with $B_{t_n}^m$ the samples of B_{t_n} , and $u_s^m = u_\theta(s, \hat{X}_n^m)$ with u_θ the control function trained by the last epoch. All the loss functions are minimized by the RMSProp algorithm. Each epoch consists of $M = 10^4$ pilot sample paths, and at the i -th iteration step, the mini-batch size is set to $|M_i| = 256$. The inner iteration steps are $J = 2K = 2$.

The neural networks u_α and v_θ both consist of 4 hidden layers with W ReLU units in each hidden layer, where the used values of W are reported in the numerical results. The adversarial network ρ_η is given by Eq. (18) with the output dimensionality $r = 600$ and $c = 100$. At the i -th iteration step, the learning rates of u_α and v_θ are both set to $\delta_0 \times 10^{-3} \times 0.01^{i/I}$, and the learning rate of ρ_η is set to $\delta_0 \times 10^{-2} \times 0.01^{i/I}$, where $\delta_0 := 3d^{-0.5}$ for $d \leq 1000$ and $\delta_0 := 3d^{-0.8}$ for $d > 1000$. All the tests are implemented by Python 3.12 and PyTorch 2.5.1. If no otherwise specified, the algorithm is accelerated by the strategy of Distributed Data Parallel (DDP) * on a compute node equipped with 8 GPUs (NVIDIA A100-SXM4-80GB).

References

- [1] Ali Al-Aradi, Adolfo Correia, Gabriel Jardim, Danilo de Freitas Naiff, and Yuri Saporito. Extensions of the deep Galerkin method. *Appl. Math. Comput.*, 430:Paper No. 127287, 18, 2022.
- [2] Achref Bachouch, Côme Huré, Nicolas Langrené, and Huyên Pham. Deep neural networks algorithms for stochastic control problems on finite horizon: numerical applications. *Methodol. Comput. Appl. Probab.*, 24(1):143–178, 2022.
- [3] Christian Beck, Sebastian Becker, Patrick Cheridito, Arnulf Jentzen, and Ariel Neufeld. Deep splitting method for parabolic PDEs. *SIAM J. Sci. Comput.*, 43(5):A3135–A3154, 2021.
- [4] Richard Bellman. *Dynamic programming*. Princeton University Press, Princeton, NJ, 1957.

*https://github.com/pytorch/tutorials/blob/main/intermediate_source/ddp_tutorial.rst

- [5] Wei Cai. DeepMartNet – a martingale based deep neural network learning algorithm for eigenvalue/BVP problems and optimal stochastic controls, 2023, arXiv:2307.11942 [math.NA].
- [6] Wei Cai, Shuixin Fang, and Tao Zhou. Soc-martnet: A martingale neural network for the hamilton-jacobi-bellman equation without explicit inf h in stochastic optimal controls, 2024, 2405.03169.
- [7] Wei Cai, Andrew He, and Daniel Margolis. DeepMartNet – a martingale based deep neural network learning method for Dirichlet BVP and eigenvalue problems of elliptic pdes, 2023, arXiv:2311.09456 [math.NA].
- [8] Weinan E, Jiequn Han, and Arnulf Jentzen. Deep learning-based numerical methods for high-dimensional parabolic partial differential equations and backward stochastic differential equations. *Commun. Math. Stat.*, 5(4):349–380, 2017.
- [9] Weinan E and Bing Yu. The deep Ritz method: a deep learning-based numerical algorithm for solving variational problems. *Commun. Math. Stat.*, 6(1):1–12, 2018.
- [10] Zhiwei Gao, Liang Yan, and Tao Zhou. Failure-informed adaptive sampling for PINNs. *SIAM J. Sci. Comput.*, 45(4):A1971–A1994, 2023.
- [11] Maximilien Germain, Huyên Pham, and Xavier Warin. Approximation error analysis of some deep backward schemes for nonlinear PDEs. *SIAM J. Sci. Comput.*, 44(1):A28–A56, 2022.
- [12] Ling Guo, Hao Wu, Xiaochen Yu, and Tao Zhou. Monte Carlo fPINNs: deep learning method for forward and inverse problems involving high dimensional fractional partial differential equations. *Comput. Methods Appl. Mech. Engrg.*, 400:Paper No. 115523, 17, 2022.
- [13] Jiequn Han, Arnulf Jentzen, and Weinan E. Solving high-dimensional partial differential equations using deep learning. *Proceedings of the National Academy of Sciences*, 115(34):8505–8510, 2018.
- [14] Jiequn Han and Jihao Long. Convergence of the deep BSDE method for coupled FBSDEs. *Probab. Uncertain. Quant. Risk*, 5:Paper No. 5, 33, 2020.
- [15] Jiequn Han, Jianfeng Lu, and Mo Zhou. Solving high-dimensional eigenvalue problems using deep neural networks: a diffusion Monte Carlo like approach. *J. Comput. Phys.*, 423:109792, 13, 2020.
- [16] Di He, Shanda Li, Wenlei Shi, Xiaotian Gao, Jia Zhang, Jiang Bian, Liwei Wang, and Tie-Yan Liu. Learning physics-informed neural networks without stacked back-propagation. In Francisco Ruiz, Jennifer Dy, and Jan-Willem van de Meent, editors, *Proceedings of The 26th International Conference on Artificial Intelligence and Statistics*, volume 206 of *Proceedings of Machine Learning Research*, pages 3034–3047. PMLR, 25–27 Apr 2023.
- [17] Pierre Henry-Labordere. Counterparty risk valuation: A marked branching diffusion approach, 2012, 1203.2369.
- [18] Pierre Henry-Labordère, Xiaolu Tan, and Nizar Touzi. A numerical algorithm for a class of bsdes via the branching process. *Stochastic Processes and their Applications*, 124(2):1112–1140, 2014.
- [19] Zheyuan Hu, Khemraj Shukla, George Em Karniadakis, and Kenji Kawaguchi. Tackling the curse of dimensionality with physics-informed neural networks. *Neural Networks*, 176:106369, 2024.

- [20] Côme Huré, Huyên Pham, Achref Bachouch, and Nicolas Langrené. Deep neural networks algorithms for stochastic control problems on finite horizon: convergence analysis. *SIAM J. Numer. Anal.*, 59(1):525–557, 2021.
- [21] Côme Huré, Huyên Pham, and Xavier Warin. Deep backward schemes for high-dimensional nonlinear PDEs. *Math. Comp.*, 89(324):1547–1579, 2020.
- [22] Shaolin Ji, Shige Peng, Ying Peng, and Xichuan Zhang. Solving stochastic optimal control problem via stochastic maximum principle with deep learning method. *J. Sci. Comput.*, 93(1):Paper No. 30, 28, 2022.
- [23] Peter E. Kloeden and Eckhard Platen. *Numerical solution of stochastic differential equations*, volume 23 of *Applications of Mathematics (New York)*. Springer-Verlag, Berlin, 1992.
- [24] Lizuo Liu, Bo Wang, and Wei Cai. Linearized learning with multiscale deep neural networks for stationary Navier-Stokes equations with oscillatory solutions. *East Asian J. Appl. Math.*, 13(3):740–758, 2023.
- [25] Ziqi Liu, Wei Cai, and Zhi-Qin John Xu. Multi-scale deep neural network (MscaleDNN) for solving Poisson-Boltzmann equation in complex domains. *Commun. Comput. Phys.*, 28(5):1970–2001, 2020.
- [26] Nikolas Nüsken and Lorenz Richter. Interpolating between BSDEs and PINNs: deep learning for elliptic and parabolic boundary value problems. *J. Mach. Learn.*, 2(1):31–64, 2023.
- [27] Bernt Øksendal. *Stochastic differential equations*. Universitext. Springer-Verlag, Berlin, sixth edition, 2003. An introduction with applications.
- [28] Huyên Pham. *Continuous-time stochastic control and optimization with financial applications*, volume 61 of *Stochastic Modelling and Applied Probability*. Springer-Verlag, Berlin, 2009.
- [29] M. Raissi, P. Perdikaris, and G. E. Karniadakis. Physics-informed neural networks: a deep learning framework for solving forward and inverse problems involving nonlinear partial differential equations. *J. Comput. Phys.*, 378:686–707, 2019.
- [30] Maziar Raissi. Forward-backward stochastic neural networks: Deep learning of high-dimensional partial differential equations, 2018, arXiv:1804.07010 [stat.ML].
- [31] Robert J. Elliott Samuel N. Cohen. *Stochastic Calculus and Applications*. Birkhäuser New York, NY, 2015.
- [32] Justin Sirignano and Konstantinos Spiliopoulos. DGM: a deep learning algorithm for solving partial differential equations. *J. Comput. Phys.*, 375:1339–1364, 2018.
- [33] Chuwei Wang, Shanda Li, Di He, and Liwei Wang. Is \hat{L}^2 physics informed loss always suitable for training physics informed neural network? In Alice H. Oh, Alekh Agarwal, Danielle Belgrave, and Kyunghyun Cho, editors, *Advances in Neural Information Processing Systems*, 2022.
- [34] Jiongmin Yong and Xun Yu Zhou. *Stochastic controls*, volume 43 of *Applications of Mathematics (New York)*. Springer-Verlag, New York, 1999. Hamiltonian systems and HJB equations.
- [35] Yaohua Zang, Gang Bao, Xiaojing Ye, and Haomin Zhou. Weak adversarial networks for high-dimensional partial differential equations. *J. Comput. Phys.*, 411:109409, 14, 2020.

- [36] Wenzhong Zhang and Wei Cai. FBSDE based neural network algorithms for high-dimensional quasilinear parabolic PDEs. *J. Comput. Phys.*, 470:Paper No. 111557, 14, 2022.
- [37] Mo Zhou, Jiequn Han, and Jianfeng Lu. Actor-critic method for high dimensional static Hamilton-Jacobi-Bellman partial differential equations based on neural networks. *SIAM J. Sci. Comput.*, 43(6):A4043–A4066, 2021.